Force Model for Complex Profile Tool in Broaching Inconel 718

Jing Ni
Hangzhou Dianzi University
Kangcheng Tong
Hangzhou Dianzi University
Zhen Meng (mengzhen0601@126.com)
Hangzhou Dianzi University https://orcid.org/0000-0003-1780-6054
Kai Feng
Hangzhou Dianzi University

Research Article

Keywords: Complex profile tool, Nickel-based superalloy, Shear zone projection, broaching model

Posted Date: June 30th, 2021

DOI: https://doi.org/10.21203/rs.3.rs-650250/v1

Force model for complex profile tool in broaching inconel 718

Jing Ni, Kangcheng Tong, Zhen Meng*, Kai Feng

School of Mechanical Engineering, Hangzhou Dianzi University, Hangzhou 310005, PR China;

Correspondence: mengzhen@hdu.edu.cn (Zhen Meng)

Corresponding author at: School of Mechanical Engineering, Hangzhou Dianzi University, No. 1158, Jianggan District, Hangzhou, 310005, Zhejiang Province, PR China.

Abstract:

Complex profile broaches are widely used in the manufacture of complex parts of aero-engines, but their cutting forces in the broaching process are difficult to predict and control. A new numerical model for broaching force with complex profile tools is presented, which considers the area and arc length of curved shear zone projection. The area and arc length were calculated by the curve function of the projection plane, which is firstly predicted by FEM simulation. Compared with the conventional force model, the accuracy of the modified model has been moderately improved. Ultimately, the modified main broaching force (Y-direction) model and the modified normal force (Z-direction) model show a significant improvement in accuracy by 4.8% and 9.7%, respectively. It suggests that the projection area of curved shear zone A_1 and the projection arc length of curved shear zone l_1 have a big impact on the broaching process. Moreover, the modified model proposed in this paper can provide guidance for the design of complex profile tools and facilitate the efficient and high-precision machining of complex parts.

Keywords: Complex profile tool, Nickel-based superalloy, Shear zone projection, broaching model

1 Introduction

Inconel 718, as a kind of nickel-base superalloy, has been widely used in the manufacture of aero-engine and gas turbine components due to its high creep strength, comprehensive mechanical properties, and cavitation resistance [1-4]. However, the excellent performance of nickel-base superalloy has also brought huge challenges to its processing and manufacturing, especially, during broaching the turbine mortises. broaching is still state of the art on account of its high toughness, high precision, and efficiency [5-6]. Nevertheless, in the processing of fir-tree profiles of the turbine disk, the excessive broaching force will bring about large deformation of the workpiece material, which will lead to the inaccuracy of the machining profile [7]. Controlling the broaching force to an appropriate value is an effective way to reduce tool wear and improve broaching quality. Therefore, it is necessary to build a more accurate cutting force prediction model in the machining process of nickel-base alloy with complex

profile tools. [8]. Additionally, the establishment of a broaching force model in the process of complex tools is of great significance to assist companies in tool design and process parameter selection [9].

As for cutting modelling of complex profile tools, a great amount of work have done by predecessors, and most of the models can be categorized as theoretical analytical model [10-11], mechanistic model [12-13], empirical model [14-15] and finite element model [16-17]. But most scholars focus on the modelling of drilling or milling tools with complex blade profiles, while few scholars pay attention to broaching. Moreover, among the very limited literature on broaching force modelling, almost all focus on the modelling of broaching tools with a straight edge (the tooth profile is straight), For example, Kamath et al. [18] calibrated the broaching force coefficient of straight edge broach with different materials such as medium carbon steel, aluminum and cast iron in broaching process. Sutherland et al. [19] modeled and verified the broaching process of keyway by oblique cutting model. Zhang et al. [20] simulated the broaching process of Inconel 718 alloy by 2D finite element method, the broaching process was numerically simulated, and the empirical model of broaching force with straight profile was established. While there is little research on cutting modelling with complex profile tools. Cla et al. [21] considered the broaching with complex profile teeth, based on the oblique cutting theory, considering geometric parameters of the complex edge profile, the broaching model was established by discretizing the blade into several small segments and then summed up. Fabre et al. [22] established a circular internal broaching force model with a complex profile through an empirical formula, in which the radial cutting force was predicted precisely. As can be seen, although a minority of scholars have paid attention to the broaching force modelling with complex edge profile, they still employ traditional models or methods to evaluate the broaching force with complex profile tool, the special mechanism of chip formation is not paid attention to. It is believed that to further improve the accuracy of the cutting force prediction model, it is necessary to consider the complicated deformation of the shear zone caused by the complex profile tool.

For model modification, heretofore, with the vigorous development of computers, the method of cutting modelling combined with finite element simulation has developed into a more mature stage. Based on the 2D finite element method, the friction data under heavy load and high temperature were introduced by Boyd et al. [23] to modify the finite element model and thus improve the modelling accuracy. Based on the Coupled Eulerian-Lagrangian (CEL) finite element model, Peng et al. [24] considered the effect of the tool flank wear on the cutting force modelling, and the flank wear of the actual tool was measured by laser scanning microscope, then the geometric model was updated in the pretreatment of the simulation, so as to improve the cutting force modelling accuracy.

According to the literature, in this paper, a novel broaching force model based on the projection area of the curved shear zone was proposed, and the 3D finite element simulation was employed to predict the area and arc length of the curved shear zone projection. Based on the experimental data, the undetermined coefficients of the traditional and modified broaching force model are fitted. And the difference between the traditional model and the proposed one are also compared.

2 Numerical broaching force model

2.1 Analysis of curved blade tool

As shown in Fig. 1 (a), during broaching the turbine mortises, the broaching process of a single tooth can be equivalent to the orthogonal cutting of the curved blade tool. When the tool is fed the depth of δ, the curved cutting edge starts to contact the workpiece, but the whole edge of the tool does not contact the workpiece simultaneously. More importantly, the contact length of the edge profile is also variable during broaching, which results in a unique shear zone morphology. At the same time, as shown in Fig. 1 (c), the projection area of curved shear zone A_1 is on the XY plane, which is perpendicular to the projection plane space shown in Fig. 1 (b). The area of the projection plane is related to broaching force, where the arc length of curved zone l_1 is also related to the broaching force. Hence, the area and arc length of the above two projection surfaces are used to characterize the cutting force.

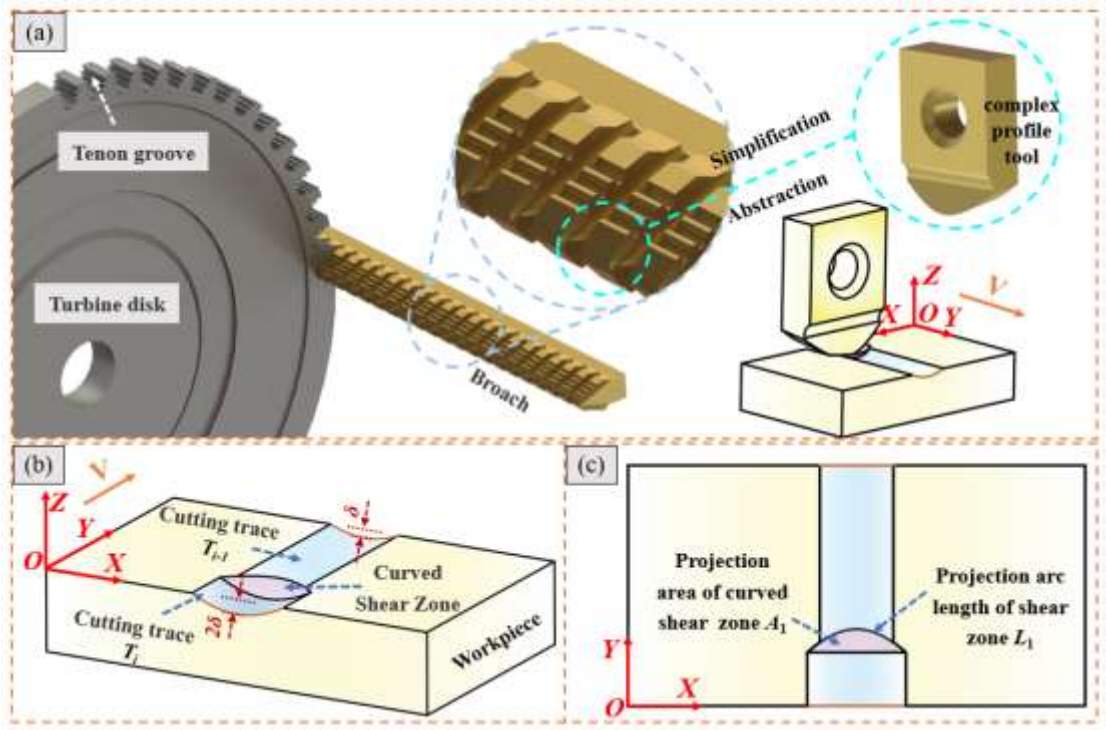

Fig.1 Schematic diagram of broaching process with complex profile tool (a) Broaching process of turbine disk; (b) Morphology of the curved shear zone; (c) Characteristics of the curved shear zone;

2.2 Broaching force modelling process

According to Altintas et al. [25], the cutting process is the coexistence of the cutting effect and blade scraping effect. Thus, the broaching force model with straight profile tool can be expressed by [21,26],

$$\begin{aligned} F_t &= k_{\mathrm{ts}} \cdot \left(b * \delta\right)^{\alpha} + k_{\mathrm{tc}} \cdot b \\ F_f &= k_{\mathrm{fs}} \cdot \left(b * \delta\right)^{\beta} + k_{\mathrm{fc}} \cdot b \end{aligned} \tag{1}$$

where, F_t and F_f are the main broaching force (Y direction) and the normal force (Z direction), respectively, b and δ are the broaching width and broaching depth, namely, the rise per tooth of the broach, as shown in Fig.2 (a); k_{ts} and k_{fs} are the specific cutting pressure of the main broaching force and the normal force, respectively, k_{tc} and k_{fc} are the edge force coefficients of the main broaching force and the normal force, α and β are constant.

As shown in Fig.2 (b), being different from the straight profile tool, the undeformed area of the complex profile tool cannot be expressed in the form of $A_s = b * h$, but the area enclosed by the edge profile, denoted as A_c. And the cutting width of complex profile tool is not constant and will change with the progressive broaching depth.

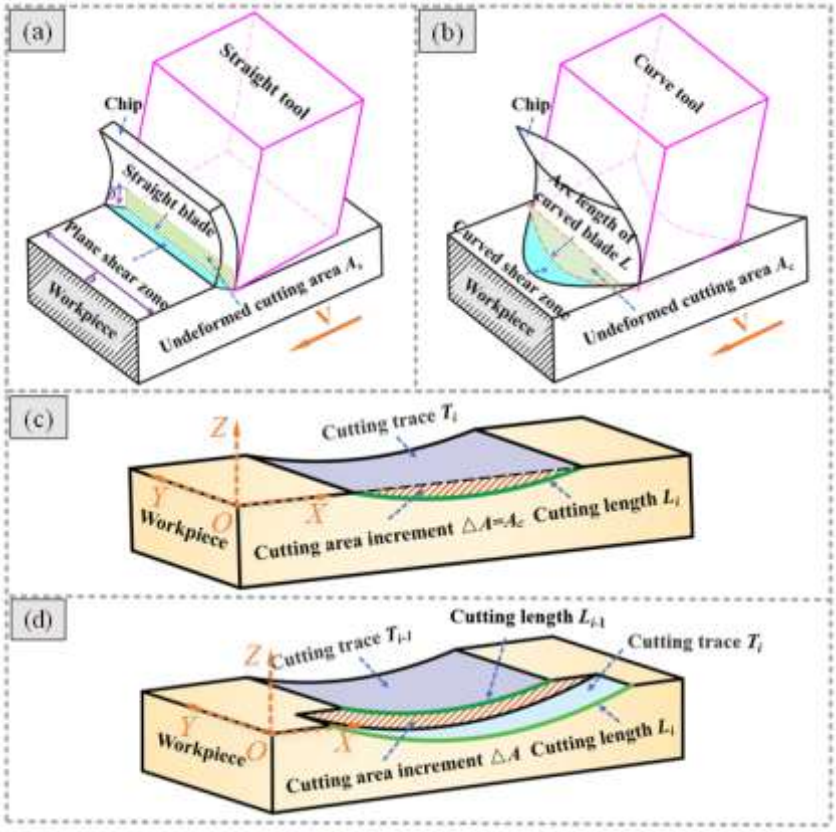

Fig.2 Schematic diagram of broaching and area increment and arc length change of complex profile tool. (a) Schematic diagram of broaching with straight profile tool; (b) Schematic diagram of broaching with complex profile tool;(c) Undeformed area and arc length of complex profile tool in first broaching; (d) Undeformed area and arc length of complex profile tool in subsequent broaching;

Stage I: modelling of the undeformed cutting area

According to the above analysis, the undeformed cutting area will vary with different broaching depths. As shown in Fig. 2(c) and (d), during the first broaching process, the undeformed area A_c is a half-period sinusoid, but for the subsequent process, due to the previous cutting trace $T_{i\text{-}1}$, the current undeformed cutting area is surrounded by two sinusoids, where the area is $\triangle A$. Additionally, one of the sinusoids offsets equidistantly by the other, and the contact arc length of the edge profile l is the arc segment where the tooth contacts the workpiece. In this paper, the profile of the tool can be expressed by

$$y=A*\sin(2*pi*x/\omega) \tag{2}$$

The undeformed cutting area can be obtained through definite integral, which can be expressed as

$$A_c = \int_{a_i}^{b_i} f_i(x) * dx - \int_{a_{i-1}}^{b_{i-1}} f_{i-1}(x) * dx \tag{3}$$

where $f_{i\text{-}1}(x)$ is the previous contacting curve between the workpiece and the tool. $f_i(x)$ is the current contacting curve.

Stage II: modelling of the conventional cutting force

Similarly, the contact length of complex profile tool can be expressed by

$$L = \int_L f(x, y) * ds = \int_L ds = \int_L \sqrt{[1 + (dy / dx)^2]} * dx \tag{4}$$

Consequently, the cutting area increment and contact length of complex profile tool changing with the number of cuts can be obtained.

According to the above analysis, the traditional broaching force model with complex profile tool can be expressed in the following form:

$$\begin{aligned} F_t &= k_{ts} \cdot A_c^{\alpha} + k_{tc} \cdot l \\ F_f &= k_{fs} \cdot A_c^{\beta} + k_{fc} \cdot l \end{aligned} \tag{5}$$

where F_t and F_f are the main broaching force (Y direction) and the normal force (Z direction), respectively, A_c is the undeformed area of the complex profile tool, l is the contact arc length of the complex profile tool.

Stage III: modelling of the modified cutting force

From Fig.2(a-b), the projection area of curved shear zone A_1 and the projection arc length of curved shear zone l_1 are both distinctive. Due to the characteristics of this unique shear zone, the chip will be seriously deformed. Different from the traditional chip with uniform thickness, the chip generated through this special shear zone is thick in the middle and thin on both sides, and the deformation resistance of the chip will cause the change of broaching force. For this reason, the modified broaching force model with the complex profile tool should be given by:

$$F_t = k_{ts} \cdot A_c^{\alpha} + k_{tc} \cdot l + k_{ts}^{'} \cdot A_1 + k_{tc}^{'} \cdot l_1$$
$$F_f = k_{fs} \cdot A_c^{\beta} + k_{fc} \cdot l + k_{fs}^{'} \cdot A_1 + k_{fc}^{'} \cdot l_1 \quad (6)$$

where k'_{ts} and k'_{fs} are the shear zone area influenced coefficient of the main broaching force and the normal force, respectively, k'_{tc} and k'_{fc} are the shear zone arc profile influenced coefficient of the main broaching force and the normal force, and the acquisition of A_1 and l_1 will be presented in the next section.

3 Prediction of the shear zone in simulation

3.1 Preprocessing of simulation

Based on the above analysis, it can be found that the area of curved shear zone A_1 and arc length of curved shear zone l_1 will be variable with feeding. To explore the chip formation and unique shear zone morphology, the broaching process simulation was realized through the 3D finite element method.

In the process of simulation, to control the elements sizes and grid nodes in the cutting area to shorten simulation time, a larger cutting depth (0.4-0.6 mm) was used, which almost does not affect the simulation accuracy. The workpiece was defined as an elastic-plastic body and was endowed with the JC constitutive model of Inconel 718, which was derived from literature [27], as listed in Table 1. Correspondingly, the tool was regarded as a rigid body, where the tool profile is defined as

$$y=3*\sin(2*pi*x) \quad (7)$$

The number of grid nodes of the workpiece was 24366, with 126108 grid elements and the local mesh size of the workpiece is 0.005mm. While relatively sparse grids could be used in the tool, where the number of grids nodes is 5046, with 26088 grid elements, the local mesh size of the tooltip is 0.2mm. Then the interaction between the tool and the workpiece was set, mainly the contact pair between the rake face and the bottom of the chip, and simultaneously the contact pair between the tool flank face and the machined surface, where the friction coefficient between the contact surfaces was set to be 0.4. For the boundary condition, the bottom of the workpiece was fixed, and the moving speed of the tool was set to 2.4 m/min, as listed in Table 2. Additionally, the simulation time is set to 0.1 s.

$$\sigma = (A + B \cdot \varepsilon^n)(1 + c \cdot \ln(\frac{\dot{\varepsilon}}{\dot{\varepsilon}_0}))(1 - (\frac{T - T_r}{T_m - T_r})^m) \quad (8)$$

Table 1 Johnson-Cook constitutive model parameters for Inconel 718

A (MPa)	B (MPa)	n	C	m	$\dot{\varepsilon}_0$ (s^{-1})	T_m (° C)	T_0 (° C)
1485	904	0.777	0.015	1.689	0.001	1800	25

Table 2 Setting parameters of the cutting simulation

Workpiece nodes	Tool nodes	Workpiece cells	Tool nodes	Broaching velocity(mm/s)	Broaching depth(mm)	Friction coefficient
24366	5046	126108	26088	40	0.4,0.5,0.6	0.4

3.2 Post processing of simulation

When the simulation was completed, the post-processing results of 0.6mm depth were extracted first, the simulation state where the chip was just about to be raised from the surface of the workpiece was captured, as shown in figure 3(a).

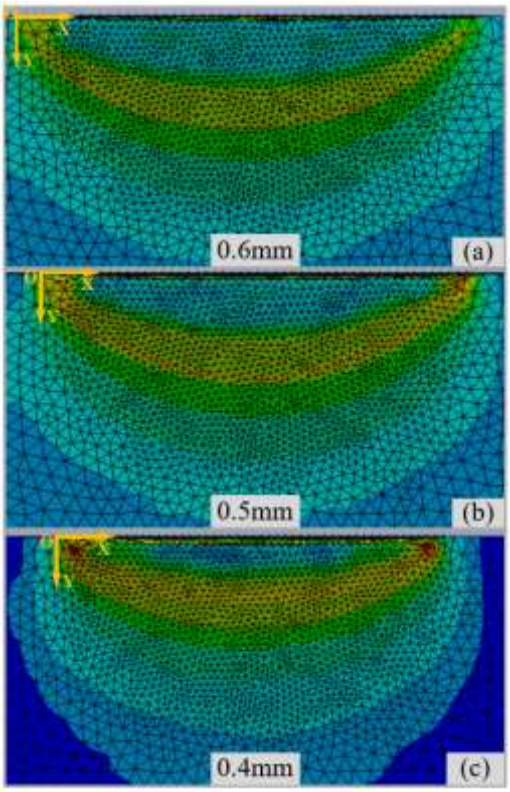

Fig.3 Morphology of the curved shear zone. (b) Morphology of shear zone at 0.6mm depth of cut; (c)Morphology of shear zone at 0.5mm depth of cut; (d)Morphology of shear zone at 0.4mm depth of cut;

Subsequently, the profile of curved shear zone of Fig.3(a) was point traced manually by CAD software, and 50 points were drawn at equal intervals starting from the origin O of each picture, to depict the contours of the shear zone, the position of the points of Fig.3 (a) in the CAD space was then derived, and the dimensional features of Fig.3 (a) was calibrated respectively, where Fig.3 (a) was 1912:6(that is, the actual size 6 mm in the simulation environment corresponds to 1912mm in the CAD space). Then the scatter points plots of the profile of the curved shear zone was drawn and a fit curve based on the sine curve was obtained, as shown in Fig.4, the blue line is the fitting curve obtained from the simulation at 0.6mm depth of cut, which can be expressed as

$$y_{S\text{-}0.6}=1.3322*\sin(2*pi*x/11.4706+6.3385) \quad (9)$$

The fitting curve based on the sinusoidal curve can depict the morphology of the shear zone well.

Hereafter, the broaching simulation at 0.5 mm and 0.4 mm depth of cut was carried out, and the similarity of the profile of the shear zone under each broaching depth was perceived, as shown in Fig. 3(b) and (c), based on the fact that the profile of curved shear zone at 0.4-0.6 mm depth of cut extended from the inside to the outside with the same profile, seemingly the ripples of water. A hypothesis that the profile of curved shear zone offset equidistantly with the progressive broaching depth was proposed. Similar to the method, the fitting plots of the profile of the curved shear zone at 0.4-0.5 mm depth of cut were obtained, as shown in Fig. 4. From top to bottom are the fitting curves of the simulated morphology of the curved shear zone where the depth of cut is 0.6mm, 0.5mm, and 0.4mm, respectively. By least squares method, the fitting curve of the simulated morphology of curved shear zone at 0.5mm depth of cut can be expressed as

$$y_{S\text{-}0.5}=1.1330*\sin(2*pi*x/10.3008+6.2081) \tag{10}$$

while the fitting curve at 0.4mm depth of cut can be expressed as

$$y_{S\text{-}0.4}=0.9270*\sin(2*pi*x/8.9695-0.3259) \tag{11}$$

These curve functions can be substituted into Eq. (3) and (4) to obtain the area and arc length.

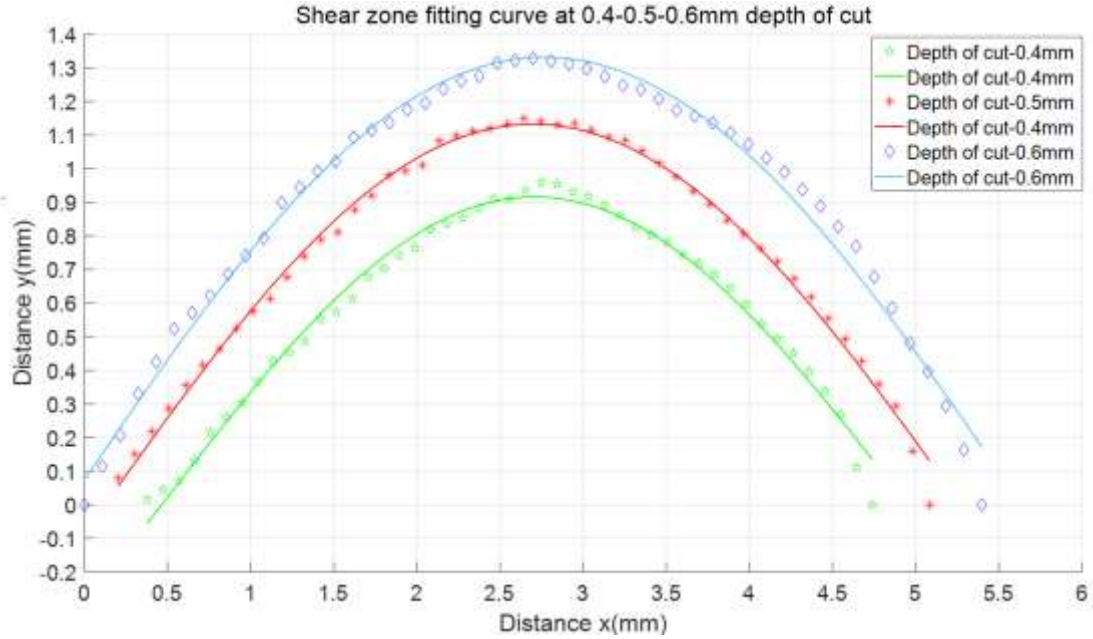

Fig.4 Simulation of shear zone fitting curve at 0.4-0.6mm depth of cut

3.3 Preliminary modelling work

According to section 2.2, based on definite integral and curve integral. The undeformed area A_c and contact arc length of the edge profile l was obtained with the progressive depth of cut, as shown in Fig.5.

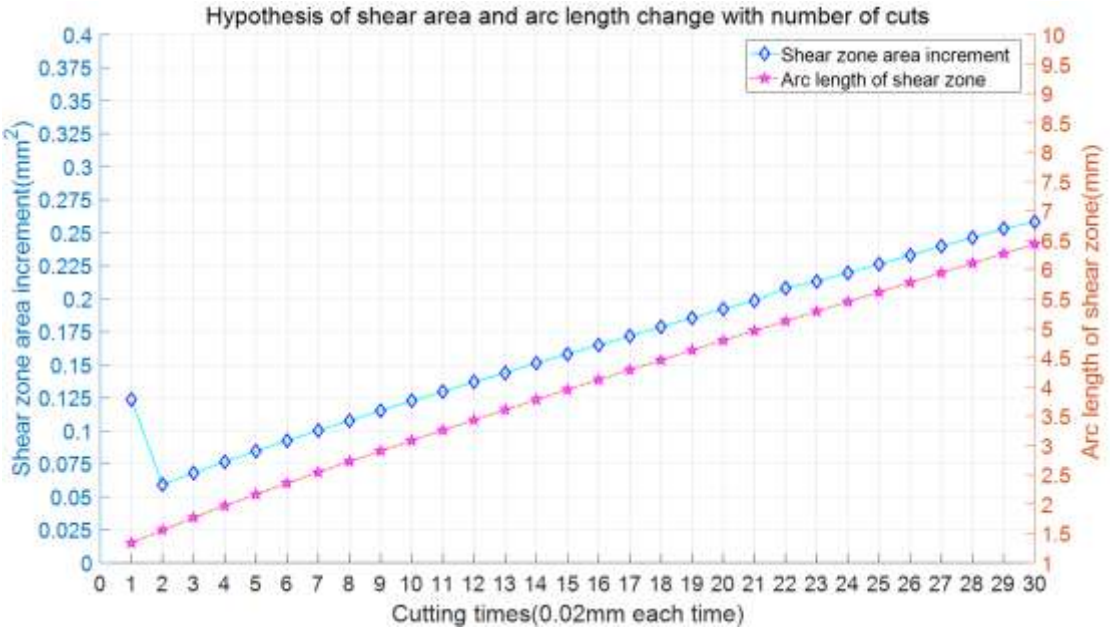

Fig.5 Theoretical cutting area and contact length change with cutting times

Based on the hypotheses aforementioned, the corresponding profile morphology of the curved shear zone at each broaching depth will be obtained based on the curve at broaching depth of 0.6mm, as shown in equation 9.

The known interval depth of simulation is 0.1mm, so the average offset of the profile can be calculated as

$$offset_{0.1} = \left(\left(1.3322 - 1.1330\right) + \left(1.1330 - 0.9270\right)\right) = 0.20458mm \tag{12}$$

It can be inferred that the offset of the profile of the curved shear zone at the interval broaching 0.02mm depth is

$$offset_{0.02} = 0.20458 / 5 = 0.04092mm \tag{13}$$

The interval is exactly about twice the change of the broaching depth. Thus, based on the curve at 0.6 mm depth of cut, the broaching depth was successively shifted down by 0. 02mm. Similar to the undeformed cutting area A and the contact length of complex profile l, the projection area of the shear zone A_1 and the projection arc length of curved shear zone l_1 were obtained by the method of definite integration and curve integration, as shown in Fig.6. For the projection area of the shear zone A_1, the situation in first broaching is slightly different from the subsequent, as shown in the schematic in the upper left corner of Fig.6, the projection area of the shear zone A_1 is the area surrounded by the profile of curved shear zone and the edge line of the workpiece. While for subsequent broaching, owing to the previous broaching trace, the current projection area $\triangle A_{1i}$ is the annular area surrounded by two profiles generated before and now, as shown in the schematic in the lower right corner of Fig.6.

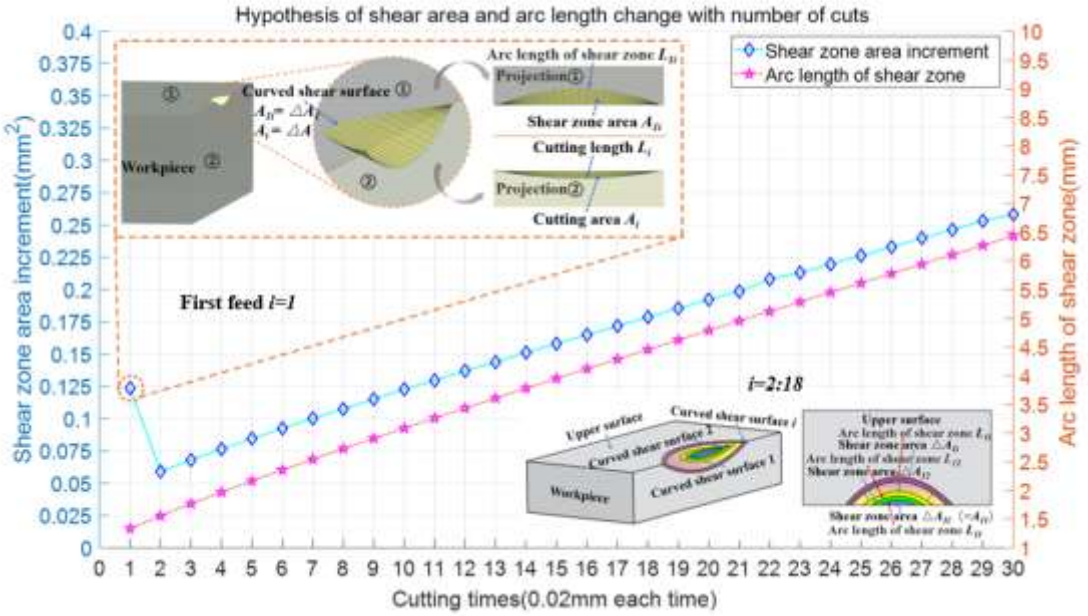

Fig.6 Projection area and arc length of shear zone change with the number of cuts

At this point, each key variable in the mechanistic model has been obtained. With the corresponding experimental data, the parameters of the model can be determined, thus the model can be established.

4 Experimental verification

4.1 Experimental device

To verify the modified broaching force model, a novel experimental system was set up, which mainly consisted of a driving slide platform, a three-dimensional dynamometer, and a cutter clamp device, as shown in Fig.7. The workpiece was fixed by a clamp, which was fixed on the three-phase force sensor by screws, and the sensor was fixed on the sliding platform and driven by a servo motor through a ball screw pair. Hereafter, the sliding platform carried the sensor and the clamping body moving at the same time with the workpiece, and the tool was fixed in place thus generating relative speed to realize broaching. The maximum output force of 4000N was provided by the servo motor through the ball screw pair.

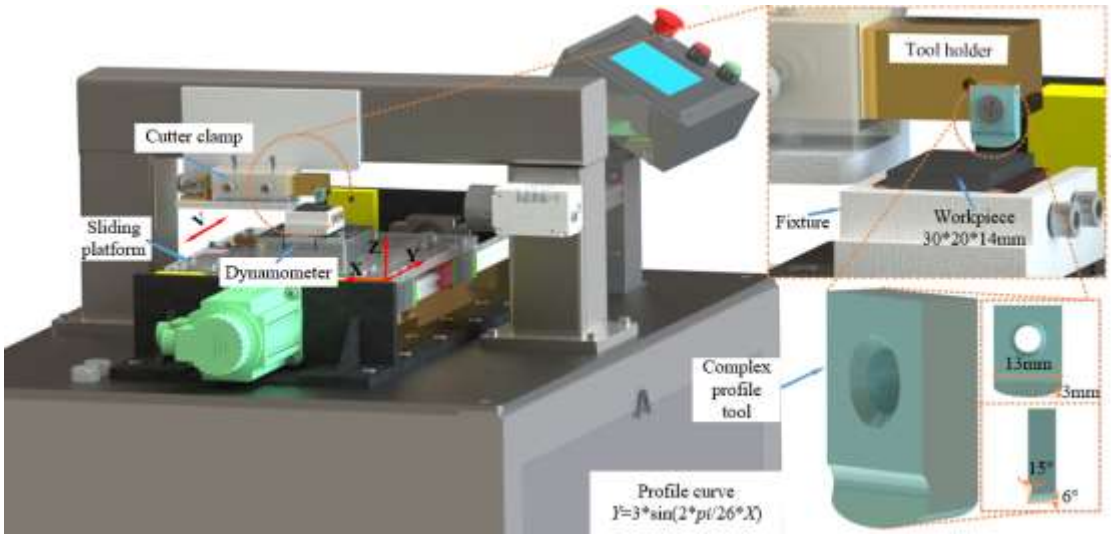

Fig.7 Experimental setup

4.2 Tool and workpiece material

The size of the workpiece was 30*20*14mm, and the material of the workpiece was nickel-based superalloy Inconel 718. The detailed composition and mechanical properties of the material are listed in Table 3 and Table 4. In this experiment, a customized tool was used, where the length of the blade of the tool is 13mm, the width is 3mm, with a 15° rake angle and 6° relief angle. The edge profile is a sinusoidal curve. It can be expressed as Eq.(7), as shown in Fig.7. The tool was made of cemented carbide, whose material composition is shown in Table 5. The hardness of the tool material reaches up to 66HRC, with high wear resistance, good toughness, and high compressive strength. As a large amount of W, CR, and V elements are dissolved in the tempered martensite after quenching, the tempered martensite maintains a high hardness, and the precipitated carbides accumulate slowly, so the tempered martensite can still maintain strength at high temperature, which enabling it to be widely used in broaching of difficult-to-cut materials.

Table 3 Chemical component of direct-aged 718

Element	Fe	Cr	Mo	Nb	Al	Ti	C	B	Ni
Mass %	18.5	19	3	5.1	0.5	0.95	0.05	0.004	rest

Table 4 The mechanical capability of inconel 718

Yield strength σ_s(MPa)	Elongation ratio δ(%)	Young's modulus E(GPa)	Thermal conductivity λ(W/mK)	Density ρ(kg/m^3)	Hardness (HRC)	Poisson's ratio μ
1200	23.3	206	11.2	8470	49	0.3

Table 5 Chemical component of W18Cr4V high-speed steel

Element	C	W	Cr	V	Mo	Si
Mass %	0.73~0.83	17.20~18.70	3.80~4.50	1.00~1.20	≤0.30	≤0.40

4.3 Experimental procedure

To calibrate coefficients in Eq.(1), the straight profile broaching experiment is carried out. As shown in Fig. 8, to change the broaching width and broaching depth simultaneously, the method of part of the blade cutting into the workpiece was adopted. The broaching speed was kept at 2.4m/min, and the values of the broaching width b and the broaching depth δ are shown in Table 6 where tests were repeated 3 times. Then, a single-factor broaching experiment with a complex profile tool was carried out with a fixed broaching speed of 2.4 m/min, and the progressive broaching depth was 0.02 mm each time,15 times of progressive broaching are completed, with a total of 0.3mm broaching depth. The details of broaching parameters can be seen in Table 7 where tests were repeated 3 times for validating dates. The progressive cutting depth of the workpiece was realized by placing a gasket at the bottom of the workpiece step by step, thus raising the workpiece by 0.02mm each time, the above process parameters are all the recommended values of actual turbine disk tenon groove broaching.

The broaching force in two directions was obtained by a ME (Type ME-K3D120) sensor with a Charge-amplifier (Type GSV-1A4) and a data acquisition system for force measurement (Type INV3018CT) connected to the computer. The experimental data were collected in real-time through utek data collection software, under a sampling frequency of 10kHz.

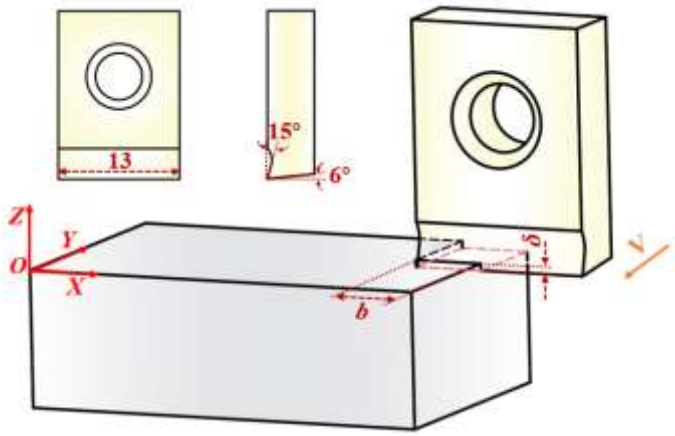

Fig.8 Schematic diagram of broaching with a straight profile tool

Table 6 Broaching parameters of the straight profile tool

No.	Broaching speed (mm/s)	Broaching width b(mm)	Broaching depth δ(mm)
1		1	0.02
2		2	0.04
3	40	3	0.06
4		4	0.08
5		5	0.10

Table 7 Broaching parameters of curved edge tool

Broaching speed (mm/s)	Single broaching depth (mm)	Total broaching depth (mm)
40	0.02	0.3

5 Results and discussion

5.1 Establishment of the traditional model and modified model

The coefficients of the main broaching force of the straight profile tool were obtained by least-square fitting, where k_{ts}, α, k_{tc} are 6441,1.20,22.02, respectively. The coefficient of determination (R) of this fitting is 0.9976, with a moderate root-mean-square error (RMSE), as shown in TS-X in Table 8, indicating a high degree of the fitting. Accordingly, these coefficients were adopted in the main broaching force model with a complex profile tool and corresponding modified model.

Then based on coefficients obtained by broaching with straight profile tool, and combined with the change law of the undeformed cutting area A_c and the contact length of complex profile l with cutting times (namely the broaching depth)obtained in section 3.3, the relationship between main broaching force with the undeformed cutting area A_c and the contact length of complex profile l can be established, namely the main broaching force model with complex profile tool, which in essence, is the modification of the main broaching force model based on the traditional model. And the information of the traditional model of the main broaching force (Y-direction) with complex profile tool is shown in TC-X in Table 8.

It can be found that directly applying the traditional model to the main broaching force model with a complex profile tool does not work well. By introducing features of the curved shear zone, the modified main broaching force model was established, where k'_{tc} and k'_{tc} are 606.5,7.89, respectively, as shown in MC-X in Table 8. Among the 15 groups of experimental data, the first 10 groups were used for fitting (broaching depth from 0.02mm to 0.20mm), and the last 5 groups were used for verification (broaching depth from 0.22mm to 0.30mm). Intuitively, it can be seen the projection area of the shear zone A_1 plays an important role in the improvement of model accuracy while the projection arc length of the shear zone l_1 almost has no effect on the model.

For the normal force, the method of model establishment is similar to the main broaching force. Firstly, the model coefficients k_{fs}, β and k_{fc} were calibrated by broaching with a straight profile tool, as shown in TS-Z in Table 8. After that, according to the above coefficients, combined with the undeformed cutting area A_c and the contact length of complex profile l, the traditional normal force model with a complex profile tool was established, as shown in TC-Z in Table 8. Ultimately, by introducing the character of the curved shear zone, the modified main broaching force model was established, where k'_{fs} and k'_{fc} are 42.47,20.74, respectively, as shown in MC-Z in Table 8. Among the 15 groups of experimental data, the first 10 groups were used for fitting (broaching depth from 0.02mm to 0.20mm), and the last 5 groups were used for

verification (broaching depth from 0.22mm to 0.30mm). It can be seen that both the undeformed cutting area A_c and the contact length of edge profile l have effects on the model accuracy, thus lower down the root-mean-square error(RMSE) of the normal force model.

Table 8 Fitting information of each model

Group	Fit type	R-square	RMSE	Coeff	*a*	*b*	*c*	*d*	*e*
TS-X	$y=a*A_c\text{^}b+c*l+d*A_1+e*l_1$	0.9976	54.29	3	6441	1.20	22.02	/	/
TC-X		0.9716	127.1	3	6441	1.20	22.02	/	/
MC-X		0.9978	49.58	5	6441	1.20	22.02	606.5	7.89
TS-Z		0.9850	39.56	3	290.7	1.46	162.1	/	/
TC-Z		0.8620	72.28	3	290.7	1.46	162.1	/	/
MC-Z		0.9848	23.96	5	290.7	1.46	162.1	42.47	20.74

5.2 Comparison of traditional model and modified model

It can be seen from the mean square error, for the main broaching force, the modified model based on the characteristics of the curved shear zone shows a huge reduction in root-mean-square error(RMSE) from 127.1 to 49.58. And the goodness of fit also shows a slight increase, which is reflected in the increase in R-square. Moreover, a set of validation data were used to test the generalization ability of the fitting. Concretely, the last five sets of experimental results were used for verification, as shown in Table 9, the maximum error of the traditional model is 264.4N, the minimum is 115.3N, and the average is 178.4N, while the maximum error of the modified model is 148.7N, the minimum is 2.8N, and the average is 62.6N, the average predicted value is 115.8N lower than that of the traditional model. And the relative error rate is selected to evaluate the fitting effect. As shown in Fig.9, the upper green line is the relative error of fitting of the traditional main broaching model with a complex profile tool while the yellow one is the modified model. The relative error rate of the traditional main broaching force model was 10.96% at the maximum and 4.78% at the minimum, correspondingly, for the modified model the maximum relative error rate is 6.16%, with the minimum relative error rate of 0.12%. Through the relative error information above, it can be concluded that compared with the traditional main broaching force model with complex profile tool, the mean error rate of the modified main broaching force model with complex profile reduces 4.8%. This suggests that the accuracy of the modified model is moderately improved compared to the traditional model, thus indicating that the features of curved shear zone such as the projection area of curved shear zone A_1 and the projection arc length of curved shear zone l_1 have a huge impact on the broaching with complex profile tool.

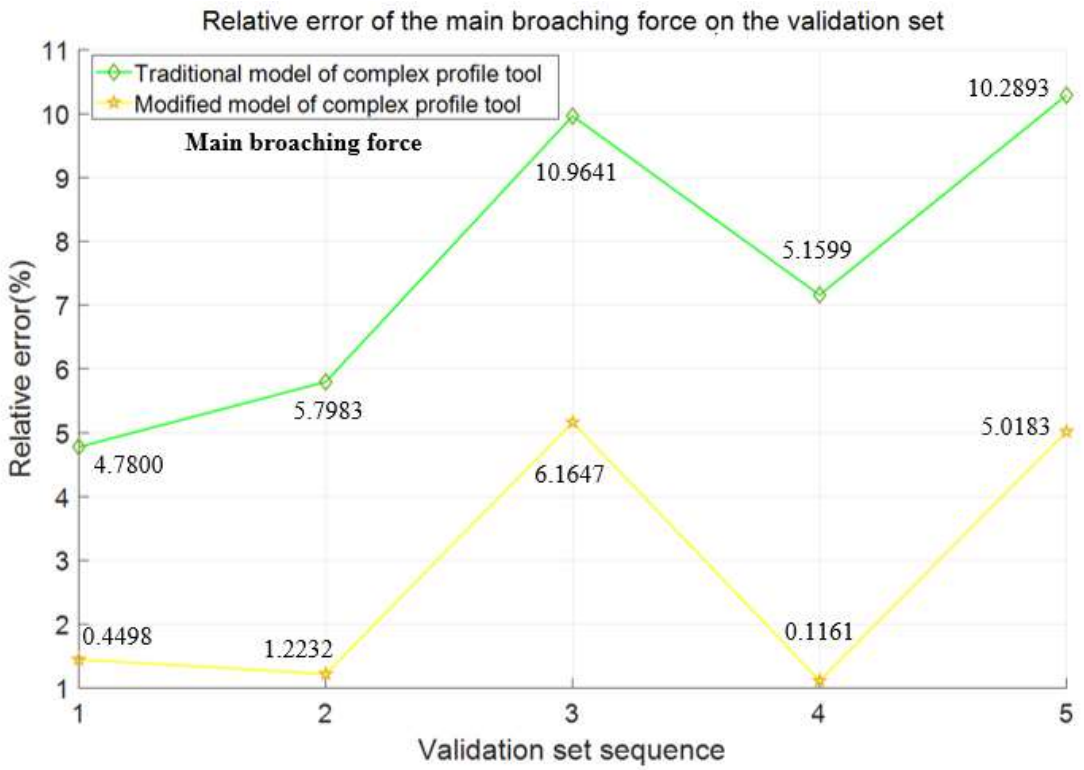

Fig.9 Relative error of the main broaching force

Table 9 Fitting results of main broaching force on the validation set

No.	Experimental data(N)	Fitting value of traditional model(N)	Fitting value of modified model (N)
1	1400.5	1285.2	1389.7
2	1607.4	1467.6	1577.9
3	1962.9	1698.5	1814.2
4	2030.4	1906.0	2027.6
5	2411.5	2163.4	2290.5

Similarly, compared with the traditional model with a complex profile tool, the root-mean-square error (RMSE) of the modified normal force based on the characteristics of the curved shear zone is greatly reduced, about a third of the traditional one. Furthermore, a set of validation data which were from the same source as the main broaching force were used to test the generalization ability of the fitting, as shown in Table 10, the maximum error of the traditional model is 138.1N, the minimum is 74.6N, and the average is 99.0N, while the maximum error of the modified model is 49.4N, the minimum is 2.5N, and the average is 19.0N, the average predicted value is 80N lower than that of the traditional model. In like manner, the relative error rate is selected to evaluate the fitting effect. As shown in Fig.10, the upper cyan line is the relative error of fitting of traditional normal force model with complex profile tool while the red one is modified, model. The relative error rate of the traditional normal force model was 16.78% at the maximum and 9.06% at the minimum, correspondingly,

for the modified model the maximum relative error rate is 6.00%, with the minimum relative error rate of 0.30%. By analysis, compared with the traditional normal force model with complex profile tool, the mean error rate of the modified normal force model with complex profile tool reduces 9.7%. It can be concluded that the accuracy of the modified model is greatly improved compared to the traditional model, thus certificating again that the features of curved shear zone such as the projection area of curved shear zone A_1 and the projection arc length of curved shear zone l_1 have a huge impact on the broaching with complex profile tool.

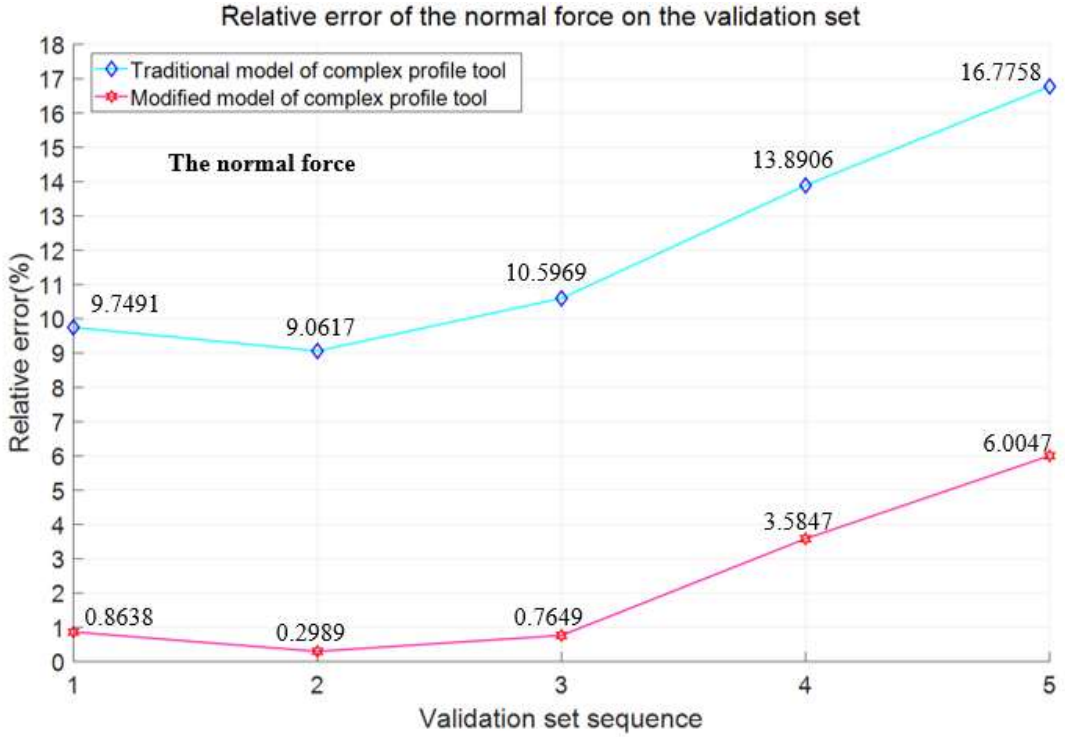

Fig.10 Relative error of the normal force

Table 10 Fitting results of the normal force on the validation set

No.	Experimental data(N)	Fitting value of traditional model(N)	Fitting value of modified model (N)
1	638.7	558.4	631.6
2	664.1	589.5	666.6
3	709.1	621.8	702.8
4	767.2	652.7	737.6
5	823.4	685.3	774.0

5 Conclusion

In this paper, a novel broaching force model with the projection of shear zone is proposed, which introduces the morphological characteristic of the curved shear zone to modify the traditional main broaching force (Y-direction) and the normal force (Z-direction) models, so as to predict the progressive broaching process of Inconel 718

with complex profile tool. At length, the effectiveness of the model is verified by comparing with the traditional broaching model. The main findings of the paper can be summarized as follows:

- The shear deformation zone when broaching with complex profile tool was explored, which is of great difference from the traditional straight profile tool. The morphology and evolution of the shear zone of the complex profile tool are studied by broaching simulation.
- Experimental results show that the projection area of curved shear zone A_1 and the projection arc length of curved shear zone L_1 were of great importance on broaching force modelling.
- Compared with the traditional broaching model, the modified model based on the curved shear zone was first introduced to predict the progressive broaching process of inconel 718 with a complex profile tool. The results show that in the direction of main broaching force (Y-direction), compared with the traditional main broaching force model with complex profile tool, the relative error rate of the modified broaching force model with complex profile tool is reduced by 4.8%, and the average predicted value is 115.8N lower than that of the traditional model. Its relative error rate in the normal force(Z-direction) is reduced by 9.7%, and the average predicted value is 80N lower than that of the traditional model. which shows the validity of the modified model. Moreover, the modified model proposed in this paper can provide guidance for the design of complex profile tools and facilitate the efficient and high-precision machining of complex parts.

6 Declarations

6.1 Funding

This research was supported by National Natural Science Foundation of China (Grant No. 51775153), China; National Natural Science Foundation of China (Grant No. 52005143),China;Science Fund for Distinguished Young Scholars of Zhejiang Province (LR20E050002), China; the National Natural Science Foundation of Zhejiang Province (Grant No. LQ21E050012), China.

6.2 Competing interests

The authors declare that they have no competing interests

6.4 Availability of data and material

The data generated during and/or analyzed during the current study are available from the corresponding author on reasonable request.

6.5 Code availability

The code generated during the current study is available from the corresponding author on reasonable request.

6.6 Ethics approval

Not applicable.

6.7 Consent to participate

Not applicable.

6.8 Consent for publish

Not applicable.

6.9 Authors'Contributions

JingNi: conceptualization, methodology, investigation, writing–original draft preparation.Kangchen Tong: conceptualization, supervision, validation, writing–reviewing and editing. Jiajun Yuan: supervision, visualization, writing–reviewing, and editing. Zhen Meng: supervision, resources, writing–reviewing, and editing. All authors read and approved the final manuscript.

7 Reference

1. Ezugwu E O, Wang Z M, Machado A R et al (1999) The machinability of nickel-based alloys: a review. Journal of Materials Processing Technology 86:1-16. https://doi.org/10.1016/S0924-0136(98)00314-8

2. Rahman M, Seah W, Teo T T et al (1997) The Machinability of Inconel 718. Journal of Materials Processing Technology 63(1):199-204.https://doi.org/10.1016/S0924-0136(96)02624-6

3. D Dudzinski, Devillez A, Moufki A et al (2004) A review of developments towards dry and high speed machining of Inconel 718 alloy. International Journal of Machine Tools & Manufacture 44(4):439-456. https://doi.org/10.1016/S0890-6955(03)00159-7

4. Arunachalam R M, Mannan M A, Spowage A C et al (2004) Surface integrity when machining age hardened Inconel 718 with coated carbide cutting tools. International Journal of Machine Tools & Manufacture 44(14):1481-1491. https://doi.org/10.1016/j.ijmachtools.2004.05.005

5. Martin S, Peng B, Andreas F B et al (2018) Model-based analysis in finish broaching of inconel 718. International Journal of Advanced Manufacturing Technology 97. https://doi.org/10.1007/s00170-018-2221-5

6. Vogtel P, Klocke F, Puls H et al (2013) Modeling of Process Forces in Broaching Inconel 718. Procedia CIRP 8:409–414. https://doi.org/10.1016/j.procir.2013.06.125

7. Sutherland J W, Salisbury E J, Hoge F W (1997) A model for the cutting force system in the gear broaching process. International Journal of Machine Tools & Manufacture 37(10):1409-1421. https://doi.org/10.1016/S0890-6955(97)00014-X

8. [1] Wang X, Li M (2020) Research on three-dimensional curved surface rolling based on rigid arc-shaped rollers. The International Journal of Advanced Manufacturing Technology 107(2). https://doi.org/10.1007/s00170-020-05096-1

9. Arrazola P J, Zel T, Umbrello D (2013) Recent advances in the modeling of metal machining processes. CIRP Annals - Manufacturing Technology 62(2):695–718. https://doi.org/10.1016/j.cirp.2013.05.006

10. W. Y, Bao (2000) Modeling micro-end-milling operations. Part I: analytical cutting force model. International Journal of Machine Tools & Manufacture. https://doi.org/10.1016/S0890-6955(00)00054-7
11. Segonds S, Masounave J, Songmene V (2013) A simple analytical model for burr type prediction in the drilling of ductile materials. Journal of Materials Processing Tech 213(6):971-977. https://doi.org/10.1016/j.jmatprotec.2012.11.030
12. Okafor A C, Sultan A A et al (2016) Development of a mechanistic cutting force model for wavy-edge bull-nose helical end-milling of inconel 718 under emulsion cooling strategy. Applied Mathematical Modelling 40(4):2637-2660. https://doi.org/10.1016/j.apm.2015.09.040
13. Srinivasa Y V, Shunmugam M S (2013) Mechanistic model for prediction of cutting forces in micro end-milling and experimental comparison.International Journal of Machine Tools & Manufacture 67:18-27. https://doi.org/10.1016/j.ijmachtools.2012.12.004
14. Vogtel P, Klocke F, Puls H (2013) Modelling of Process Forces in Broaching Inconel 718. Procedia CIRP 8:409–414. https://doi.org/10.1016/j.procir.2013.06.125
15. I Biró, Szalay T (2017) Extension of empirical specific cutting force model for the process of fine chip-removing milling.The International Journal of Advanced Manufacturing Technology 88(9):2735-2743.https://doi.org/10.1007/s00170-016-8957-x
16. Sahoo P, Patra K, Singh V K (2020) Influences of TiAlN coating and limiting angles of flutes on prediction of cutting forces and dynamic stability in micro milling of die steel (P-20). Journal of Materials Processing Technology 278:116500. https://doi.org/10.1016/j.jmatprotec.2019.116500
17. Afazov S M, Ratchev S M, Segal J (2010) Modelling and simulation of micro-milling cutting forces. Journal of Materials Processing Tech 210(15):2154-2162. https://doi.org/10.1016/j.jmatprotec.2010.07.033
18. Kamath R C, Kuttan A (2009) Determination of proportionality constants from cutting force modelling experiments during broaching operation. International Journal of Science & Technology 3(02). https://www.researchgate.net/publication/289299901_Determination_of_proportionality_constants_from_cutting_force_modelling_experiments_during_broaching_operation
19. Sutherland J W, Salisbury E J, Hoge F W et al (1997) A model for the cutting force system in the gear broaching process.International Journal of Machine Tools & Manufacture 37(10):1409-1421. https://doi.org/10.1016/S0890-6955(97)00014-X
20. Zhang Y L, Chen W Y (2012) Finite Element Modelling of the Broaching Process of Inconel718. Materials science forum 697-698:p.39-43.

https://www.researchgate.net/publication/271962432_Finite_Element_Modelling_of_the_Broaching_Process_of_Inconel718
21. Cla B, Gf A, Gp A (2019) A geometrical and mechanistic generalized model for complex shape broaching of super alloy.Procedia CIRP 82(C):461-466. https://doi.org/10.1016/j.procir.2019.04.042
22. Fabre D, Bonnet C, Mabrouki T (2020) Modelling of macroscopic cutting forces in internal broaching of an X12Cr13 stainless steel.Proceedings of the Institution of Mechanical Engineers Part B.Journal of Engineering Manufacture 234(11). https://doi.org/10.1177/0954405420911262
23. Boyd J M, Hosseinkhani K, Veldhuis S C et al (2016) Improved prediction of cutting forces via finite element simulations using novel heavy-load,high-temperature tribometer friction data.International Journal of Advanced Manufacturing Technology 86:2037-2045. https://doi.org/10.1007/s00170-015-8284-7
24. Peng B, Bergs T, Klocke F (2019) An advanced FE-modelling approach to improve the prediction in machining difficult-to-cut material.The International Journal of Advanced Manufacturing Technology. https://doi.org/10.1007/s00170-019-03456-0
25. Y. Altintas (2000) Manufacturing automation: metal cutting mechanics, machine tool vibrations, and CNC design / 2nd. Cambridge university press. https://www.emerald.com/insight/content/doi/10.1108/ir.2004.04931aae.003/full/html
26. E Zlü, Araghizad A E, Budak E et al (2020) Broaching tool design through force modelling and process simulation.CIRP Annals - Manufacturing Technology 69(1). https://doi.org/10.1016/j.cirp.2020.04.035
27. Klocke, F.Lung, D.Buchkremer et al (2013) Inverse identification of the constitutive equation of In 718 and AISI 1045 from FE machining simulations.14th Corp Conference on Modelling of Machining Operations. https://doi.org/10.1016/j.procir.2013.06.091